41st AIAA Fluid Dynamics Conference and Exhibit
27 - 30 June 2011, Honolulu, Hawaii

AIAA 2011-3098

Investigation of Co-Flow Jet Airfoil Mixing Mechanism Using Large Eddy Simulation

Hong-Sik IM [*], Ge-Cheng Zha[†], Bertrand P.E. Dano[‡]
Dept. of Mechanical and Aerospace Engineering
University of Miami
Coral Gables, Florida 33124
E-mail: gzha@miami.edu

Abstract

This paper uses large eddy simulation (LES) to investigate Co-Flow Jet (CFJ) airfoil flows at high angle of attack (AOA). The standard Smagorinsky model with Van Driest damping is employed to resolve the subgrid scale stress. The 5th order WENO scheme is used for the reconstruction of the inviscid flux and the 4th order central differencing for the viscous flux. The momentum coefficient(C_μ) is chosen as a parameter to control the jet flow of the CFJ airfoil. LES simulations were carried out for the different momentum coefficients. The LES results at 30^o AOA are compared with the experiment to understand the flow structure of the jet mixing and flow separation. The numerically captured qualitative flow structures are very similar to those obtained in experiment. The quantitative prediction of lift and drag agree very well with experiment.

1 Introduction

The CFJ flow control airfoil[1, 2, 3, 4] for lift enhancement and drag reduction is designed with an injection slot near leading edge and a suction slot near trailing edge. The jet having high energy is injected tangentially near leading edge and the same amount of mass flow is sucked in near trailing edge to form a zero-net mass-flux flow control. The transport of energy from the jet to the main flow allows the main flow to overcome a severe adverse pressure gradient and remain attached at high angle of attack. The high energy jet induces high circulation and hence generates high lift. The energized main flow fills the wake and therefore reduces drag. At low angle of attack, the drag reduction is often so great that a thrust or negative drag is created. The CFJ airfoil appears to be a very promising flow control technique to provide a drastic performance enhancement with the lowest energy expenditure[5].

One challenge for numerical simulation of CFJ flow control airfoil using Reynolds averaged Navier-Stokes (RANS) model is that both C_L and C_D are significantly under-predicted at high angle of attack when the jet is not strong enough and the flow is separated. Wang and Zha[6] improves the prediction at high angle of attack by using Detached Eddy Simulation(DES), which is a hybrid turbulence modeling using RANS near walls within boundary layers and large eddy simulation (LES) away from the walls. However, the lift and drag are still significantly under-predicted.

LES is an intermediate approach between the direct numerical simulation (DNS) of turbulence flows and the solution of RANS. DNS has largely been limited to simple geometries at low Reynolds number since it requires grid points $\simeq Re^{9/4}$ and times steps $\simeq Re^{3/4}$ to resolve all scales of turbulence[7]. In LES momentum and energy transfer of the large energy-carrying structures is computed directly and

---

[*] Graduate Student, AIAA Member

[†] Associate Professor, AIAA Senior Member

[‡] Adjunct Faculty, AIAA Member

only the effect of the smallest scales of turbulence is modeled. A general model for small scale structures is more plausible to obtain for LES.

LES has been used for airfoil stall flows[8, 9, 10]. For example, Moreau et al.[10] employed LES to simulate the trailing edge flow and noise of NACA0012 airfoil at near stall. It is pointed out that RANS fails to capture the stall point, while LES provides a more realistic behavior and qualitatively resolves better the shear-layer and the von Karman instabilities[10].

Recently, the experiments of the CFJ airfoil was performed to investigate the CFJ airfoil mixing process[11]. The flow visualization was achieved by using Digital Particle Image Velocimetry and also the aerodynamic forces including lift and drag were measured. In this study LES is applied to simulate the flow field of the CFJ airfoil experiment,which is AOA of 30^o and the jet momentum coefficient(C_μ) of 0.15. To better understand the jet effect, LES for lower $C_\mu = 0.08$ is also performed.

The purpose of this research are two folds: 1) using LES to further improve the prediction of lift and drag of CFJ airfoil at high angle of attack; 2)using LES to study the fundamental mixing mechanism of the CFJ airfoil. A low diffusion E-CUSP scheme[12] is used with 5th order WENO reconstruction scheme for the inviscid flux and 4th order central differencing for the viscous flux[13]. The standard Smagorinsky model with Van Driest damping is used to model the subgrid-scale stress. The high scalability parallel algorithm[14] is used. The lift and drag predicated by LES agree very well with the experiment.

2 Spatially Filtered Compressible Navier-Stokes Equations

The spatial filtering eliminates the small scale high frequency components of the fluid motion, while keeping the unsteadiness associated with the large scale turbulent motion. For an arbitrary function $u(x_i, t)$, the filtered variable $\bar{u}(x_i, t)$ is defined as:

$$\bar{u}(x_i, t) = \int_D G(x_i - \xi_i, \Delta) u(\xi_i, t) d\xi_i \tag{1}$$

where G is the filter function and Δ is the filter width and is associated with the mesh size. Similar to the case of RANS, for compressible flows, it is convenient to introduce the Farve-filtered variable $\tilde{u}(x_i, t)$ as:

$$\tilde{u}(x_i, t) = \frac{\overline{\rho u}}{\bar{\rho}} \tag{2}$$

A variable can be thus decomposed into its Favre-filtered component and fluctuating component as:

$$u(x_i, t) = \tilde{u}(x_i, t) + u''(x_i, t) \tag{3}$$

Applying these definitions and following the derivation of Knight et al.[15], the filtered compressible Navier-Stokes(NS) equations in Cartesian coordinates can be expressed as:

$$\frac{\partial \mathbf{Q}}{\partial t} + \frac{\partial \mathbf{E}}{\partial x} + \frac{\partial \mathbf{F}}{\partial y} + \frac{\partial \mathbf{G}}{\partial z} = \frac{1}{Re}(\frac{\partial \mathbf{R}}{\partial x} + \frac{\partial \mathbf{S}}{\partial y} + \frac{\partial \mathbf{T}}{\partial z}) \tag{4}$$

where

$$\mathbf{Q}=\begin{pmatrix}\bar\rho\\ \bar\rho\tilde u\\ \bar\rho\tilde v\\ \bar\rho\tilde w\\ \bar\rho\tilde e\end{pmatrix},\mathbf{E}=\begin{pmatrix}\bar\rho\tilde u\\ \bar\rho\tilde u^2+\bar p\\ \bar\rho\tilde u\tilde v\\ \bar\rho\tilde u\tilde w\\ (\bar\rho\tilde e+\bar p)\tilde u\end{pmatrix},\mathbf{F}=\begin{pmatrix}\bar\rho\tilde v\\ \bar\rho\tilde v\tilde u\\ \bar\rho\tilde v^2+\bar p\\ \bar\rho\tilde v\tilde w\\ (\bar\rho\tilde e+\bar p)\tilde v\end{pmatrix},\mathbf{G}=\begin{pmatrix}\bar\rho\tilde w\\ \bar\rho\tilde w\tilde u\\ \bar\rho\tilde w\tilde v\\ \bar\rho\tilde w^2+\bar p\\ (\bar\rho\tilde e+\bar p)\tilde w\end{pmatrix}$$

$$\mathbf{R}=\begin{pmatrix}0\\ \bar\tau_{xx}+\sigma_{xx}\\ \bar\tau_{xy}+\sigma_{xy}\\ \bar\tau_{xz}+\sigma_{xz}\\ Q_x\end{pmatrix},\mathbf{S}=\begin{pmatrix}0\\ \bar\tau_{yx}+\sigma_{yx}\\ \bar\tau_{yy}+\sigma_{yy}\\ \bar\tau_{yz}+\sigma_{yz}\\ Q_y\end{pmatrix},\mathbf{T}=\begin{pmatrix}0\\ \bar\tau_{zx}+\sigma_{zx}\\ \bar\tau_{zy}+\sigma_{zy}\\ \bar\tau_{zz}+\sigma_{zz}\\ Q_z\end{pmatrix}$$

The overbar denotes a regular filtered variable as given in eq. (1), and the tilde is used to denote the Favre filtered variable defined in eq. (2). In above equations, ρ is the density, u, v, w are the Cartesian velocity components in x, y, z directions, p is the static pressure, and e is the total energy per unit mass.

The $\bar\tau$ is the molecular viscous stress tensor and is estimated as:

$$\bar\tau_{ij}=\frac{2}{3}\tilde\mu\frac{\partial\tilde u_k}{\partial x_{\ k}}\delta_{ij}+\tilde\mu\left(\frac{\partial\tilde u_i}{\partial x_j}+\frac{\partial\tilde u_j}{\partial x_i}\right),\quad i,j=1,2,3 \tag{5}$$

The above equation is in the tensor form, where the subscript 1, 2, 3 represent the coordinates, x, y, z and the Einstein summation convention is used. The molecular viscosity $\tilde\mu=\tilde\mu(\tilde T)$ is determined by Sutherland law.

The σ is the subgrid-scale(SGS) stress tensor due to the filtering process and is expressed as:

$$\sigma_{ij}=-\bar\rho(\widetilde{u_iu_j}-\tilde u_i\tilde u_j) \tag{6}$$

The energy flux Q is expressed as:

$$Q_i=\tilde u_j(\bar\tau_{ij}+\sigma_{ij})-\bar q_i+\Phi_i \tag{7}$$

where Φ is the subscale heat flux:

$$\Phi_i=-C_p\bar\rho(\widetilde{u_iT}-\tilde u_i\tilde T) \tag{8}$$

The $\bar q_i$ is the molecular heat flux:

$$\bar q_i=-\frac{\tilde\mu}{(\gamma-1)Pr}\frac{\partial a^2}{\partial x_i}$$

where $a=\sqrt{\gamma R\tilde T}$ is the speed of sound. The equation of state as a constitutive equation relating density to pressure and temperature is defined as

$$\bar\rho\tilde e=\frac{\bar p}{(\gamma-1)}+\frac{1}{2}\bar\rho(\tilde u^2+\tilde v^2+\tilde w^2)+\rho k \tag{9}$$

where γ is the ratio of specific heats, ρk is the subscale kinetic energy per unit volume.

$$\rho k=\frac{1}{2}\bar\rho(\widetilde{u_iu_i}-\tilde u_i\tilde u_i)=-\frac{1}{2}\sigma_{ii} \tag{10}$$

The closure of equation (4) requires a model for the subgrid-scale stress, σ_{ij} and heat flux, Φ_{ij}. Most subgrid scale models employ the eddy viscosity($\tilde{\mu}_t$) approach to avoid solving additional equations. In this study, the standard Smagorinsky model with Van Driest damping[16] is used to model the subgrid-scale stress. With the Smagorinsky model, the eddy viscosity is written as

$$\tilde{\mu}_t = \bar{\rho} C_s l^2 \sqrt{2 S_{ij} S_{ij}} \tag{11}$$

where C_s is the Smagorinsky constant, l is the model length scale. In this study, the value 0.2 was used for C_s, and

$$l = (\Delta)^{1/3} \sqrt{(1 - \exp(-y^+/26))^3}$$

where Δ is the volume of the cell. S_{ij} is the rate-of-strain tensor.

In generalized coordinates(ξ, η, ζ), the governing Eq.(4) can be expressed as the following conservative form:

$$\frac{\partial Q}{\partial t} + \frac{\partial E}{\partial \xi} + \frac{\partial F}{\partial \eta} + \frac{\partial G}{\partial \zeta} = \frac{1}{Re} \left(\frac{\partial R}{\partial \xi} + \frac{\partial S}{\partial \eta} + \frac{\partial T}{\partial \zeta} \right) \tag{12}$$

where Re is the Reynolds number. The conservative variable vector Q, the inviscid flux vectors E, F, G, and the viscous fluxs R, S, T are expressed as

$$Q = \frac{1}{J} \begin{pmatrix} \bar{\rho} \\ \bar{\rho}\tilde{u} \\ \bar{\rho}\tilde{v} \\ \bar{\rho}\tilde{w} \\ \bar{\rho}\tilde{e} \end{pmatrix}, E = \begin{pmatrix} \bar{\rho} U \\ \bar{\rho}\tilde{u} U + l_x \bar{p} \\ \bar{\rho}\tilde{v} U + l_y \bar{p} \\ \bar{\rho}\tilde{w} U + l_z \bar{p} \end{pmatrix}, F = \begin{pmatrix} \bar{\rho} V \\ \bar{\rho}\tilde{u} V + m_x \bar{p} \\ \bar{\rho}\tilde{v} V + m_y \bar{p} \\ \bar{\rho}\tilde{w} V + m_z \bar{p} \end{pmatrix}, G = \begin{pmatrix} \bar{\rho} W \\ \bar{\rho}\tilde{u} W + n_x \bar{p} \\ \bar{\rho}\tilde{v} W + n_y \bar{p} \\ \bar{\rho}\tilde{w} W + n_z \bar{p} \end{pmatrix}$$

$$R = \begin{pmatrix} 0 \\ l_k \bar{\tau}_{xk} \\ l_k \bar{\tau}_{yk} \\ l_k \bar{\tau}_{zk} \\ l_k \left(\tilde{u}_i \bar{\tau}_{ki} - \bar{q}_k \right) \end{pmatrix}, S = \begin{pmatrix} 0 \\ m_k \bar{\tau} u_{xk} \\ m_k \bar{\tau}_{yk} \\ m_k \bar{\tau} u_{zk} \\ m_k \left(\tilde{u}_i \bar{\tau}_{ki} - \bar{q}_k \right) \end{pmatrix}, T = \begin{pmatrix} 0 \\ n_k \bar{\tau}_{xk} \\ n_k \bar{\tau}_{yk} \\ n_k \bar{\tau}_{zk} \\ n_k \left(\tilde{u}_i \bar{\tau}_{ki} - \bar{q}_k \right) \end{pmatrix}$$

where U, V and W are the contravariant velocities in ξ, η, ζ directions, and defined as follows.

$$U = l_t + \mathbf{l} \bullet \mathbf{V} = l_t + l_x \tilde{u} + l_y \tilde{v} + l_z \tilde{w} \tag{13}$$

$$V = m_t + \mathbf{m} \bullet \mathbf{V} = m_t + m_x \tilde{u} + m_y \tilde{v} + m_z \tilde{w} \tag{14}$$

$$W = n_t + \mathbf{n} \bullet \mathbf{V} = n_t + n_x \tilde{u} + n_y \tilde{v} + n_z \tilde{w} \tag{15}$$

where l_t, m_t and n_t are the components of the interface contravariant velocity of the control volume in ξ, η and ζ directions respectively. $\mathbf{l}$, $\mathbf{m}$ and $\mathbf{n}$ denote the normal vectors located at the centers of ξ, η and ζ interfaces of the control volume with their magnitudes equal to the surface areas and pointing to the directions of increasing ξ, η and ζ. J is the Jacobian of the transformation.

3 Implicit Time Integration

The time dependent governing equation (12) is solved using the dual time stepping method suggested by Jameson[17]. A pseudo temporal term $\frac{\partial Q}{\partial \tau}$ is added to the governing Eq. (12). This term vanishes at the end of each physical time step, and has no influence on the accuracy of the solution. An implicit pseudo time marching scheme using line Gauss-Seidel line relaxation is employed to achieve high convergence rate instead of using the explicit scheme as given by Jameson in [17]. The physical temporal term is discretized implicitly using a three point 2nd order accuracy, backward differencing as the following:

$$\frac{\partial \mathbf{Q}}{\partial t} = \frac{3\mathbf{Q^{n+1}} - 4\mathbf{Q^{n}} + \mathbf{Q^{n-1}}}{2\Delta t} \tag{16}$$

where $n-1$, n and $n+1$ are three sequential time levels, which have a time interval of Δt. The first-order Euler scheme is used to discretize the pseudo temporal term. The semi-discretized equations of the governing equations are finally given as the following:

$$\begin{gathered}\left[\left(\tfrac{1}{\Delta\tau} + \tfrac{1.5}{\Delta t}\right) I - \left(\tfrac{\partial R}{\partial \mathbf{Q}}\right)^{n+1,m}\right] \delta\mathbf{Q^{n+1,m+1}} \\ = R^{n+1,m} - \tfrac{3\mathbf{Q^{n+1,m}} - 4\mathbf{Q^{n}} + \mathbf{Q^{n-1}}}{2\Delta t}\end{gathered} \tag{17}$$

where the $\Delta\tau$ is the pseudo time step, and R is the net flux discretized in space. The Low Diffusion E-CUSP (LDE) Scheme[18, 12] is used to evaluate the inviscid flux with the 5th order WENO scheme[19, 20] and the 4th order central differencing is used for the viscous flux[19, 20].

4 Boundary Conditions

Steady state freestream conditions are used for the upstream portion of the farfield boundary. The Reynolds number based on freestream velocity and chord length is 1.19179×10^5. The freestream Mach number tested in the experiment is 0.03, but the Mach number used in the computation is 0.05. The reason is to avoid the convergence stiffness. The experiment indicates that all the non-dimensional performance coefficients including lift and drag are insensitive to the Mach number in that Mach number range. For downstream farfield boundary, the static pressure was specified as freestream value, and the streamwise gradients of other variables were forced to vanish. The periodic boundary condition is used in spanwise direction. The wall treatment suggested in [19, 20] to achieve the flux conservation by shifting half interval of the mesh on the wall is employed. The no slip condition is employed on the airfoil surface, for computing the flux $F_{1/2}$ on the wall, there is

$$G_w = \begin{pmatrix} \rho V \\ \rho u V + p\eta_x \\ \rho v V + p\eta_y \\ \rho w V + p\eta_z \\ (\rho e + p) V \end{pmatrix}_w = \begin{pmatrix} 0 \\ p\eta_x \\ p\eta_y \\ p\eta_z \\ 0 \end{pmatrix}_w$$

and a third-order accuracy wall boundary formula is used to evaluate $p|_w$,

$$p_w = \frac{1}{6}(11p_1 - 7p_2 + 2p_3)$$

At the injection cavity, total pressure and total temperature are specified, whereas the static pressure is given at the suction cavity. To achieve zero net mass flux with the CFJ flow control, the mass flow that exits the injection slot must equal the mass flow entering the suction slot. This is achieved by adjusting the total pressure in the injection cavity and the static pressure in the suction cavity. The process is iterated throughout the simulation until the desired value is reached. In the present LES simulations, the difference of the mass flow rates for injection and suction is within 2%.

5 LES Mesh

The CFJ airfoil modified from NACA6415 airfoil and tested by Dano et al.[11] is shown in Fig.1. The chord length of the airfoil is 0.3048m and the design span is 0.5906. Fig. 2 and 3 show the LES mesh for CFJ at 30^o AOA. The computation mesh is constructed using the O-mesh topology in order to improve the mesh quality around airfoil. The mesh points of 451 is placed around airfoil; total 301 points on suction surface, 151 points on the pressure surface. 211 points were used to construct mesh normal to the airfoil, and 61 points were placed in the spanwise direction. The farfield boundary locates 75 times chord from the CFJ center chord. The wing span(h) of 0.15 times chord(C) is used in this study. Total mesh size is 7913835, and partitioned to 135 blocks for the parallel computation. To represent accurately the turbulence structures in the near-wall region, the first grid point is modeled to satisfy y^+ less than unity. By the same token, Δx^+ and Δz^+ are also less than 40 over the CFJ airfoil. Δx and Δz have almost equal size over the CFJ airfoil as presented in Fig. 4 since the isotropic mesh elements are desirable for LES.

6 Jet Momentum Coefficient, C_μ

With the CFJ airfoil, C_μ is used as an important parameter for jet mass flow control. The jet momentum coefficient, a dimensionless parameter that includes mass flow rate and jet velocity, is defined as

$$C_\mu = \frac{\dot{m}_j V_j}{\frac{1}{2}\rho_\infty {V_\infty}^2 S} \tag{18}$$

where $\dot{m}_j$ is CFJ injection mass flow rate, V_j represents the injection jet velocity, the subscript $_\infty$ denotes freestream of the CFJ airfoil, and S is the airfoil planform area. In this paper two different momentum coefficients, $C_\mu = 0.008$ and $C_\mu = 0.15$ are studied.

7 Lift and Drag Calculation

The momentum and pressure at the injection and suction slots produce a reactionary force, which is automatically measured by the force balance in wind tunnel testing. However, for CFD simulation, the full reactionary force is difficult to obtain unless the complete internal ducts of injection and suction are simulated. Using control volume analysis, the reactionary force can be calculated using the flow parameters at the injection and suction slot opening surfaces[2]. Zha et al.[2] give the following formulations to calculate the lift and drag due to the jet reactionary force for a CFD simulation. By considering the effects of the injection and suction jets on the CFJ airfoil, the expressions for these reactionary forces are given as[2]:

$$\begin{aligned} F_{x_{cfj}} &= (\dot{m}_{j1}V_{j1} + p_{j1}A_{j1}) * cos(\theta_1 - \alpha) - \gamma(\dot{m}_{j2}V_{j2} + p_{j2}A_{j2}) * cos(\theta_2 + \alpha) \\ F_{y_{cfj}} &= (\dot{m}_{j1}V_{j1} + p_{j1}A_{j1}) * sin(\theta_1 - \alpha) + \gamma(\dot{m}_{j2}V_{j2} + p_{j2}A_{j2}) * sin(\theta_2 + \alpha) \end{aligned} \tag{19}$$

where the subscripts 1 and 2 stand for the injection and suction respectively, and θ_1 and θ_2 are the angles between the injection and suction slot's surface and a line normal to the airfoil chord. α is the angle of attack. γ denotes the suction coefficient; if no suction, then γ equals 0.

The total lift and drag on the airfoil can then be expressed as:

$$D = R'_x - F_{x_{cfj}} \tag{20}$$

$$L = R'_y - F_{y_{cfj}} \tag{21}$$

where R'_x and R'_y are the surface integral of pressure and shear stress in x (drag) and y (lift) direction excluding the internal ducts of injection and suction. For the CFD simulation, the total lift and drag are calculated using Eqs.(20) and (21).

8 Results and Discussion

For the unsteady LES simulation, the physical time step 0.025 with CFL number of 3 is applied. The unsteady simulations start from the initial flow field using a few hundred steps of steady state calculation. The residual is typically reduced by three orders of magnitude in each physical time step. In this paper, LES is conducted for the flows at AoA=30° and C_μ =0.15 and 0.08. Under these conditions, the flows are massively separated due to high angle of attack and weak co-flow jets. The mass flow between the injection and the suction cavity is balanced within 2%. All the LES results presented in this paper are plotted at the center span(0.075 h).

The lift and drag coefficient predicted by LES is plotted with the experiment in Fig. 5 and 6 for $C_\mu = 0.15$. The LES under-predicts the lift and drag coefficient by 7.8% and 1.7% respectively. This is a remarkable improvement compared to the DES prediction of a separated CFJ airfoil flow with lift and drag under-predicted by 22% and 64% [6]. The accurate prediction of the drag coefficient is particularly significant since drag is usually more difficult to predict than lift.

Fig. 7 shows the instantaneous flow field for C_μ=0.08 and 0.15 with velocity magnitude contour at $\bar{t} = 550T$ predicted by LES. The massive flow separations are captured with the flow structures qualitatively similar to the experimental flow visualization as shown in Fig. 8[11]. Contours of vorticity at $\bar{t} = 550T$ for $C_\mu = 0.08$ and $C_\mu = 0.15$ are shown in Fig. 9. Since vorticity is the fluid quantity that stands for the degree of fluid particle rotation, high vorticity is observed in the coflow jet region due to the flow mixing.

The time averaged and instantaneous flow field of the CFJ airfoil colored by velocity magnitude for $C_\mu = 0.15$ are shown in Fig. 10. The time averaged velocity vector field also predicts the upstream flow strip between two counter rotating vertical shear layer shown in Fig. 11 obtained from the experiment[11]. LES predicts that the coflow jet is fully attached to the CFJ suction surface and the flow in the outer shear layer is mixed into the coflow jet. The attached coflow jet as captured by the flow visualization in Fig. 8 is not shown due to the difficulty in PIV measurement near the wall boundary layer. The saddle point captured by the LES instantaneous velocity vector filed is located at about same position as the experiment. In Fig. 12, the velocity vector indicates how the outer shear is sucked into the attached coflow jet on suction surface.

The vorticity near the injection slot is illustrated in Fig. 13. Fig. 14 shows a large structure vortex field using VDA(vortex detection algorithm) near leading edge of the CFJ airfoil. VDA suggested by Graftiaux et al.[21] is used to describe the vortical structure of the flow field. The flow near the injection slot predicted by the LES has similar vortical structure compared to the experiment.

Fig. 15 shows turbulent kinetic energy(k) near the CFJ airfoil injection slot for $C_\mu = 0.15$ and $C_\mu = 0.08$. The kinetic energy for $C_\mu = 0.15$ is stronger than $C_\mu = 0.08$ due to the jet increase. Fig. 16 represents turbulent kinetic energy for $C_\mu = 0.15$ obtained by the experiment. The experiment and the LES at $C_\mu = 0.15$ show high turbulent kinetic energy after the injection and in the upper strip of the main flow.

Fig. 17, 18, and 19 show the distributions of turbulent kinetic energy at 0.15C, 0.75C, and 1 chord downstream. The axial plane at 0.15C is located between the injection slot and the saddle point, and at 0.75C is located around the suction slot near trailing edge. At 0.15C, turbulent kinetic energy for $C_\mu = 0.15$ is larger than $C_\mu = 0.08$. However, intensity of turbulence kinetic energy for $C_\mu = 0.15$

becomes smaller than $C_\mu = 0.008$ further downstream in the wake region. It indicates that when jet momentum coefficient is increased, the wake flow turbulence intensity is decreased due to the smaller separation region.

Fig. 20 shows the instantaneous streamlines in the shear flow mixing region with the attached coflow jet. The shear flow does not mix with the coflow jet for $C_\mu = 0.08$, resulting in less flow sucked into the suction cavity. The mixed flow for $C_\mu = 0.15$ is well sucked into the suction cavity.

Fig. 21, Fig. 22, and Fig. 23 represent the streamwise, shear, and lateral Reynolds stress at 0.25, and 1 chord downstream for $C_\mu = 0.15$ and $C_\mu = 0.08$ respectively. Overall, the streamwise and shear Reynolds stress are overall similar. However, the lateral Reynolds stress $(v'v')$ for $C_\mu = 0.15$ is a little larger than $C_\mu = 0.08$.

9 Conclusions

The flow mixing under a large main flow separation of the CFJ airfoil at 30^o AOA is investigated using the LES. For the jet momentum coefficient of $C_\mu = 0.15$, the LES simulation is compared with the experiment. For comparison, LES for a smaller C_μ of 0.08 is also conducted. The present LES accurately predicts lift and drag of the CFJ airfoil and shows high similarity of the flow structures compared with the experiment. The LES predicts the upstream flow strip between two counter rotating vertical shear layer and the saddle point observed in experiment. As a result of flow mixing, increased jet intensity enhances mixing in the injection region and reduce the turbulence intensity in the wake region.

Acknowledgments

This research is supported under ARO/AFOSR Grant 50827-RT-1SP.

References

[1] G.-C. Zha, B. Carroll, C. Paxton, A. Conley, A. Wells, "High Performance Airfoil with Co-Flow Jet Flow Control," *AIAA Journal*, vol. 45, 2007.

[2] G. Zha, W. Gao, and C.D. Paxton, "Jet Effects on Co-Flow Jet Airfoil Performance," *AIAA Journal*, vol. 45, pp. 1222–1231, 2007.

[3] G. Zha, and C.D. Paxton, "A Novel Flow Control Method for Airfoil Performance Enhancement Using Co-Flow Jet," *Applications of Circulation Control Technologies, AIAA Book Series, Progress in Aeronautics and Astronautics*, vol. Vol. 214, Chapter 10, pp. 293–314, 2006.

[4] G.-C. Zha, C. Paxton, A. Conley, A. Wells, nd B. Carroll, "Effect of Injection Slot Size on High Performance Co-Flow Jet Airfoil," *AIAA Journal of Aircraft*, vol. 43, pp. 987–995, 2006.

[5] D. Dano, G.-C. Zha and M. Castillo, "Experimental Study of Co-Flow Jet Airfoil Performance Enhancement Using Discrete Jets." 49th AIAA Aerospace Sciences Meeting including the New Horizons Forum and Aerospace Exposition, 4-7 Jan. 2011, Orlando, Florida, AIAA-2011-941.

[6] B.-Y. Wang, and G.-C. Zha, "Detached-Eddy Simulation of a Co-Flow Jet Airfoil at High Angle of Attack." AIAA Paper 2009-4015, to appear in Journal of Aircraft, 2011.

[7] S.A. Orszag, "Analytical Theories of Turbulence," *Journal of Fluid Mechanics*, vol. 41, pp. 363–386, 1970.

[8] I. Mary, “Large eddy simulation of vortex breakdown behind a delta wing,” *Int. J. of Heat and Fluid Flow*, vol. 24, pp. 596–605, 2003.

[9] S. Eisenbach, and R. Friedrich, “Large-eddy simulation of flow separation on an airfoil at a high angle of attack and $Re = 10^5$ using Cartesian grids,” *Theor. Comput. Fluid Dyn.*, vol. 22, pp. 213–225, 2008.

[10] S. Moreau, J. Christopher, M. Roger, “LES of the Trailing-edge Flow and Noise of a NACA0012 Airfoil Near Stall.” Proceedings of the Summer Program 2008, Center for Turbulence Research, 2008.

[11] D. Dano, D. Kirk, and G.-C. Zha, “Experimental Investigation of Jet Mixing Mechanism of Co-Flow Jet Airfoil.” AIAA-2010-4421, 2010.

[12] G.-C. Zha, Y.-Q. Shen, and B.-Y. Wang, “An improved low diffusion E-CUSP upwind scheme,” *Journal of Computer & Fluids*, vol. 48, pp. 214–220, 2011.

[13] Y.-Q. Shen, G.-Z. Zha, X.-Y. Chen , “High order conservative differencing for viscous terms and the application to vortex-induced vibration flows,” *Journal of Computational Physics*, vol. 228, pp. 8283–8300, 2009.

[14] B.-Y. Wang and G.-C. Zha, “A General Sub-Domain Boundary Mapping Procedure For Structured Grid CFD Parallel Computation,” *AIAA Journal of Aerospace Computing, Information, and Communication*, vol. 5, No.11, pp. 2084–2091, 2008.

[15] D. Knight, G. Zhou, N. Okong, and V. Shulka, “Compressible Large Eddy simulation Using Unstructured Grids.” AIAA Paper 98-0535, 1998.

[16] J.S. Samagorinsky, “General circulation experiements with the primitive equations, part I: The basic experiments.” Monthly Weather Review, Vol 91, pp.99-152, 1963.

[17] A. Jameson, “Time Dependent Calculations Using Multigrid with Applications to Unsteady Flows Past Airfoils and Wings.” AIAA Paper 91-1596, 1991.

[18] G.C. Zha, Y.Q. Shen, and B.Y. Wang, “Calculation of Transonic Flows Using WENO Method with a Low Diffusion E-CUSP Upwind Scheme.” AIAA Paper 2008-0745, 46th AIAA Aerospace Sciences Meeting, Reno, NV, Jan. 2008.

[19] Y.Q. Shen, B.Y. Wang, and G.C. Zha, “Implicit WENO Scheme and High Order Viscous Formulas for Compressible Flows .” AIAA Paper 2007-4431, 2007.

[20] Y.-Q. Shen, G.-C. Zha, X.-Y. Chen, “ High Order Conservative Differencing for Viscous Terms and the Application to Vortex-Induced Vibration Flows,” *Journal of Computational Physics*, vol. 228(2), pp. 8283–8300, 2009.

[21] L. Graftieaux, M. Michard, and N. Grosjean, “Combining PIV, POD and vortex identification algorithms for the study of unsteady turbulent swirling flows,” *Meas. Sci. Technol.*, vol. 12, pp. 1422–1429, 2001.

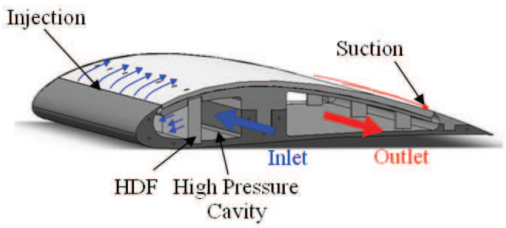

Figure 1: CFJ airfoil concept

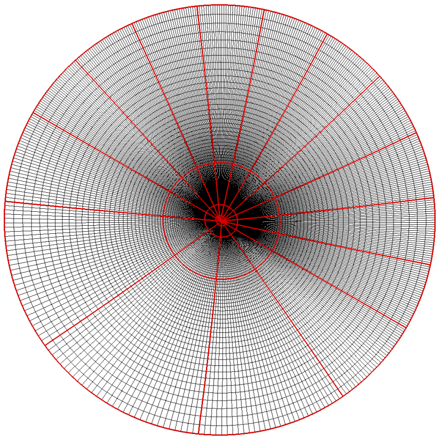

Figure 2: LES mesh for the CFJ airfoil at 30^o AOA, total mesh = 7913835, h(span)=0.15C(chord)

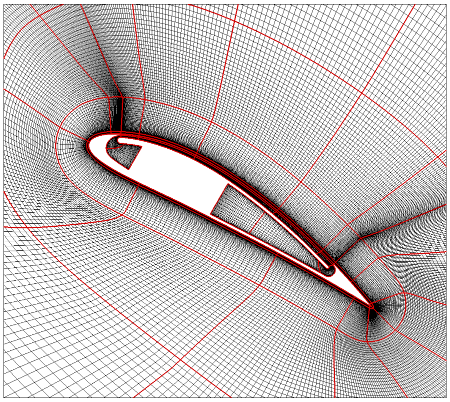

Figure 3: LES mesh around the CFJ airfoil at 30^o AOA

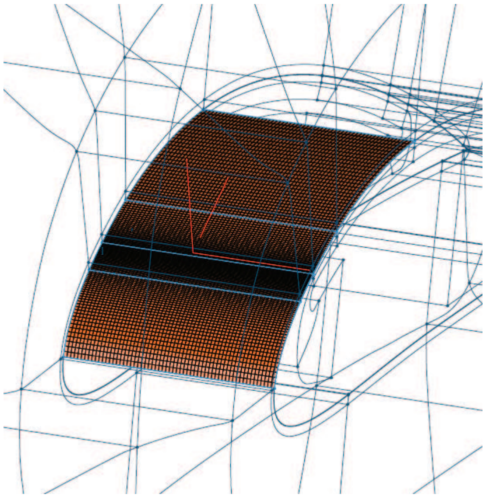

Figure 4: LES mesh on the suction surface of the CFJ airfoil at 30^o AOA

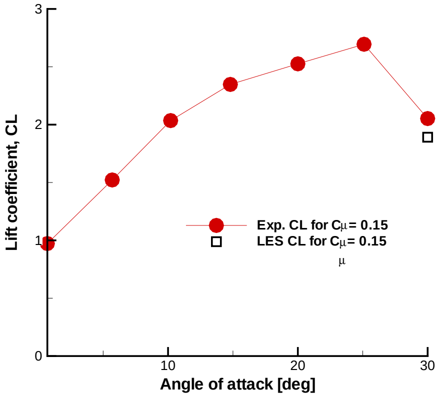

Figure 5: Predicted lift(C_L) coefficients of the CFJ airfoil at 30^o AOA

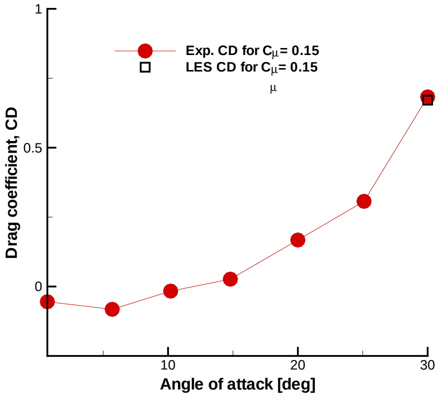

Figure 6: Predicted drag(C_D) coefficients of the CFJ airfoil at 30^o AOA

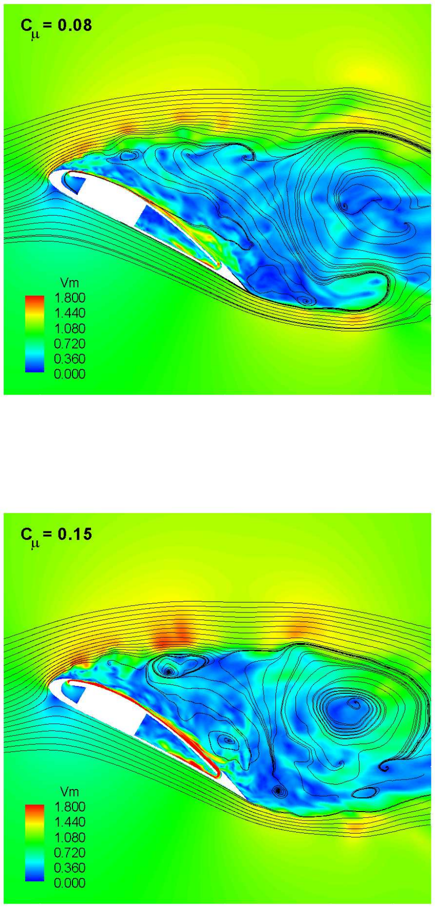

Figure 7: Instantaneous streamlines of the CFJ airfoil with velocity magnitude contour predicted by LES; AOA=30^o, $C_\mu = 0.08$(top), $C_\mu = 0.15$(bottom)

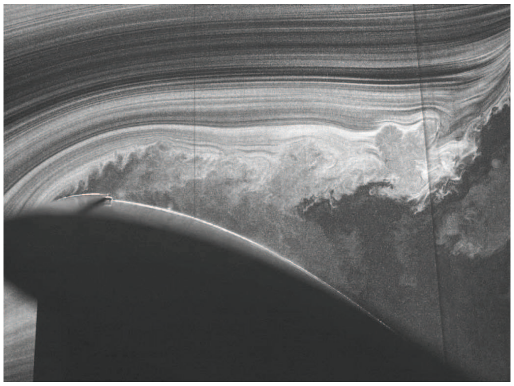

Figure 8: Instantaneous smoke visualization of the CFJ airfoil by experiment; AOA=30^o, $C_\mu = 0.15$(bottom)

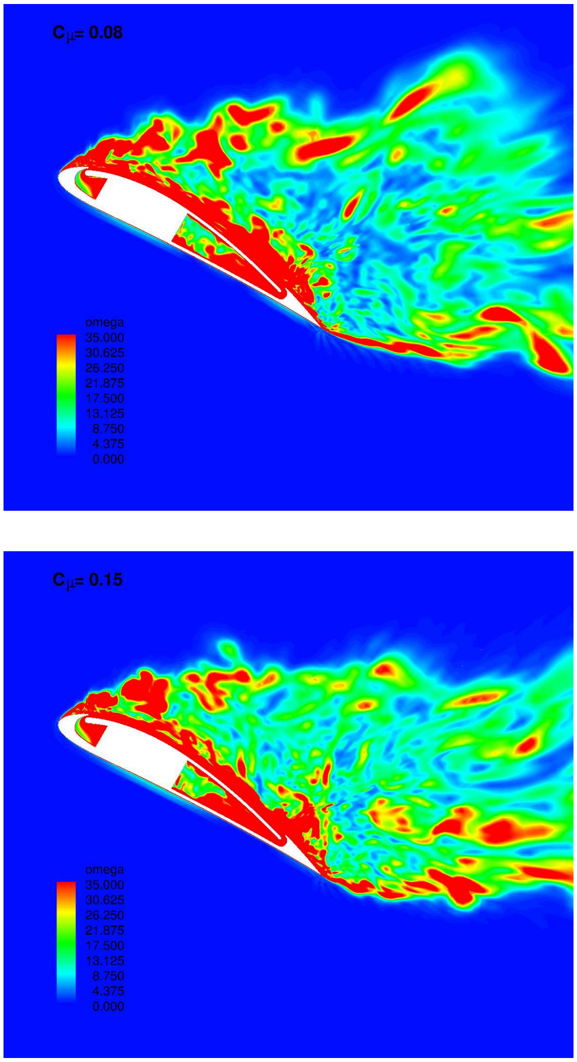

Figure 9: Instantaneous vorticity of the CFJ airfoil predicted by LES; AOA=30^o, $C_{mu} = 0.08$(top), $C_{mu} = 0.15$(bottom)

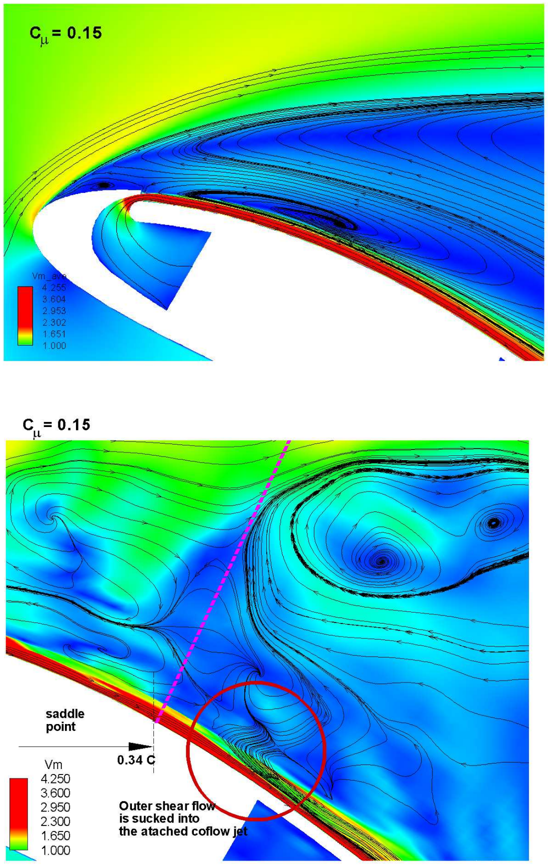

Figure 10: Contours of velocity magnitude and streamlines of the CFJ airfoil for $C_\mu = 0.15$ predicted by LES; AOA=30^o, time averaged(top), Instantaneous(bottom)

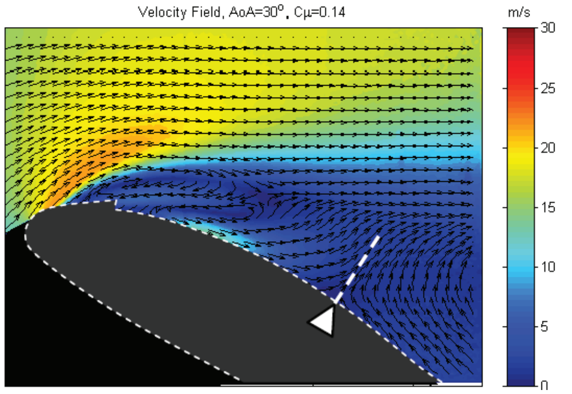

Figure 11: Time average velocity field of the CFJ airfoil by experiment; AOA=30^o, $C_\mu = 0.15$

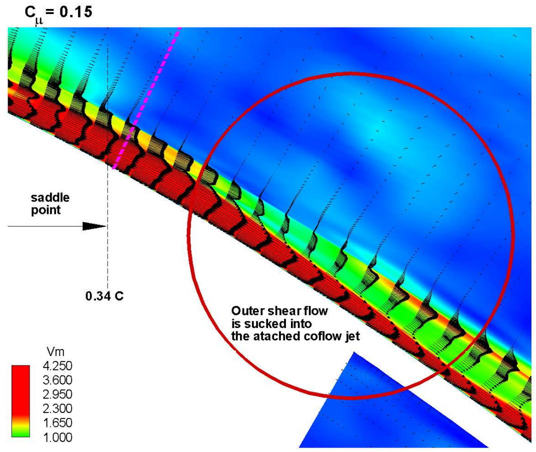

Figure 12: Instantaneous velocity vector near the saddle point predicted by LES; AOA=30^o, $C_\mu = 0.15$

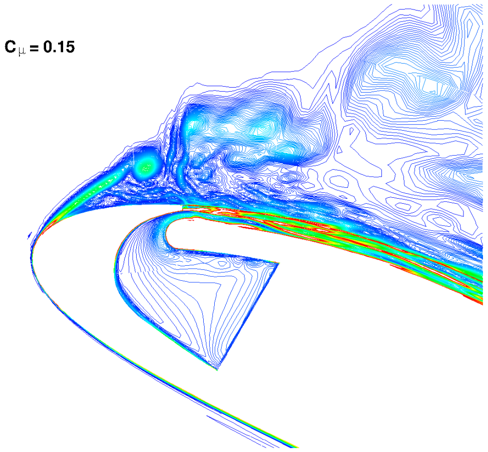

Figure 13: Instantaneous vorticity near the injection slot of the CFJ airfoil predicted by LES; AOA=30^o, $C_\mu = 0.15$

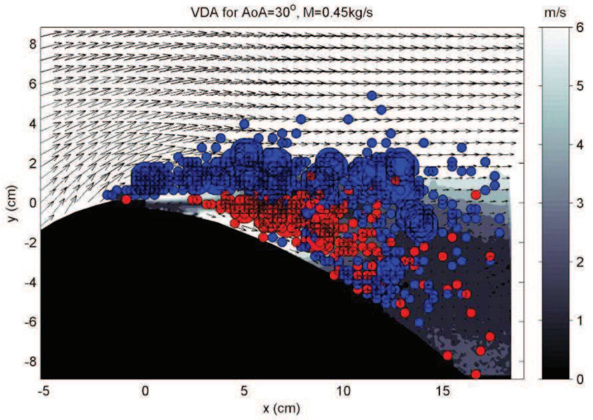

Figure 14: Time averaged VDA(vortex detection algorithm) field near the CFJ leading edge by experiment; AOA=30^o, $C_\mu = 0.15$

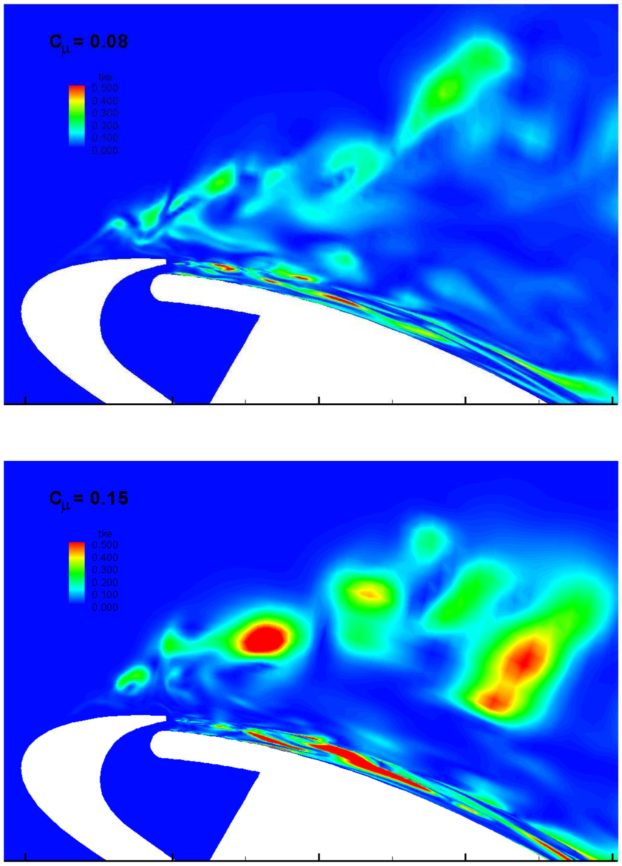

Figure 15: Contours of turbulent kinetic energy(k) near the CFJ airfoil injection slot predicted by LES; AOA=30^o, $C_\mu = 0.08$(top), $C_\mu = 0.15$(bottom)

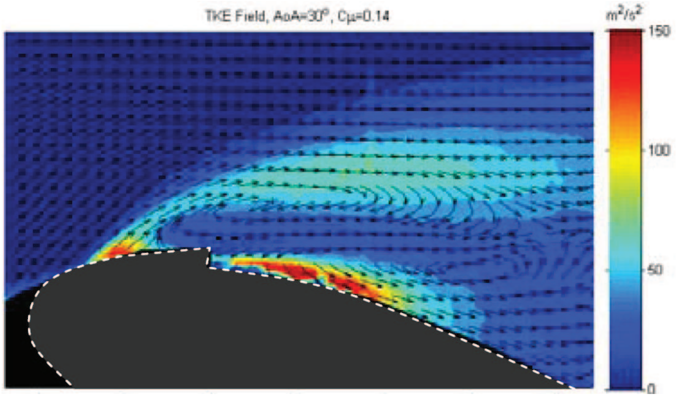

Figure 16: Contours of turbulent kinetic energy(k) near the CFJ airfoil injection slot predicted by the experiment; AOA=30^o, $C_\mu = 0.15$(bottom)

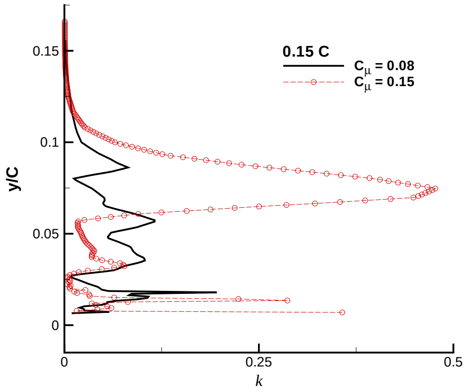

Figure 17: Distributions of turbulent kinetic energy(k) of the CFJ airfoil at 0.15C axial plane predicted by LES

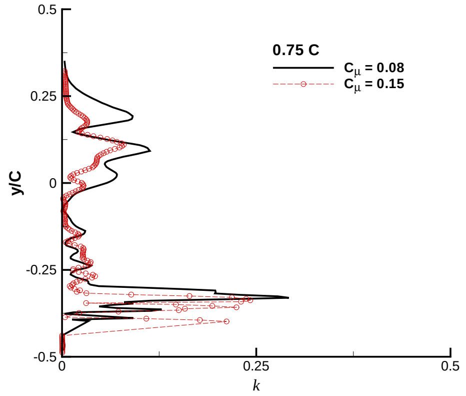

Figure 18: Distributions of turbulent kinetic energy(k) of the CFJ airfoil at 0.75C axial plane predicted by LES

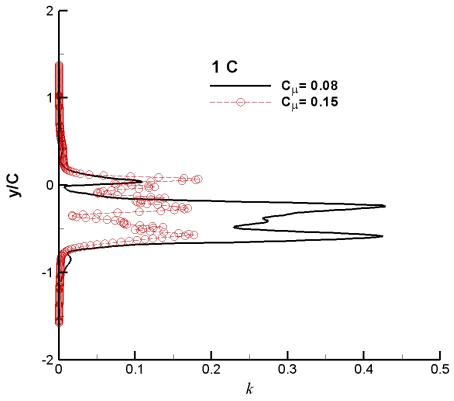

Figure 19: Distributions of turbulent kinetic energy(k) of the CFJ airfoil at 1 chord downstream predicted by LES

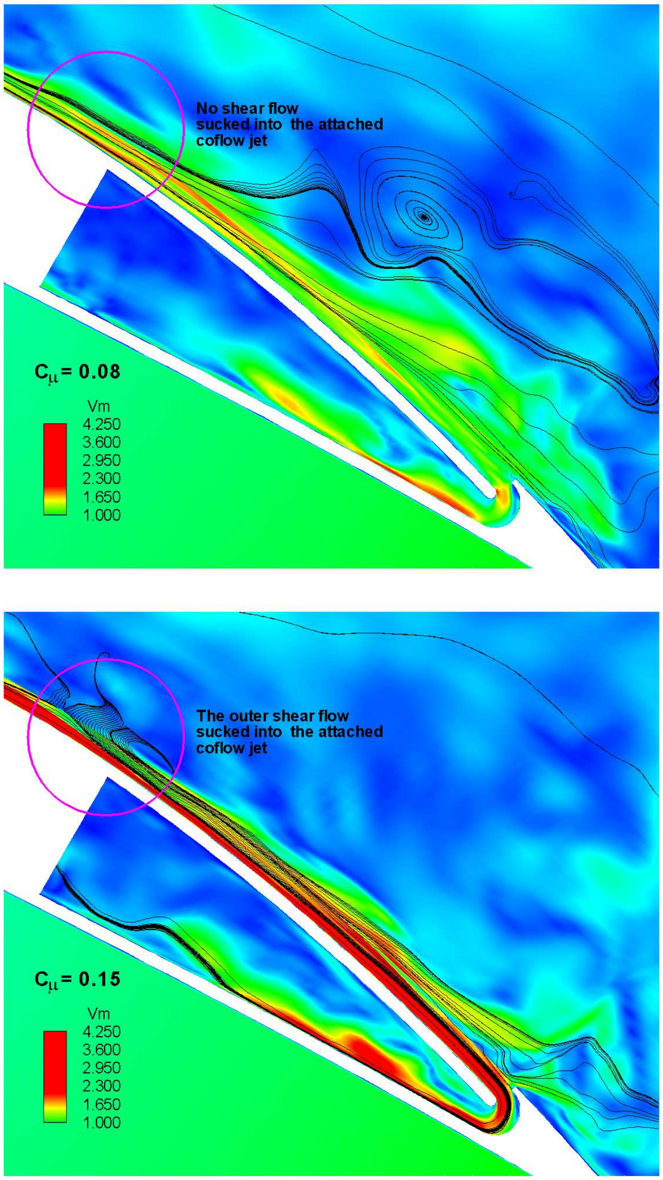

Figure 20: Instantaneous streamlines indicating mixing of the outer shear flow with the attached coflow jet predicted by LES; AOA=30^o, $C_{mu} = 0.08$(top), $C_{mu} = 0.15$(bottom)

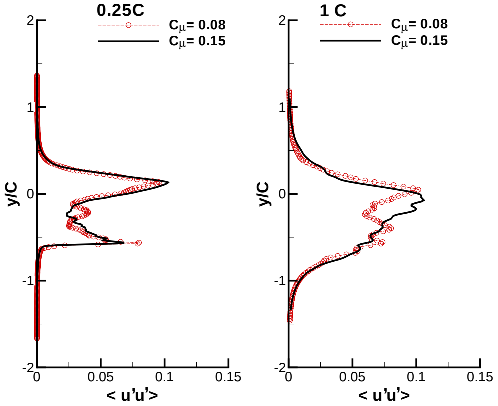

Figure 21: Streamwise Reynolds stress of the CFJ airfoil at 30^o AOA predicted by LES

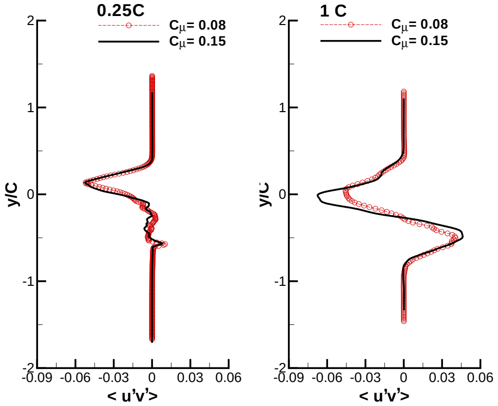

Figure 22: Shear Reynolds stress of the CFJ airfoil at 30^o AOA predicted by LES

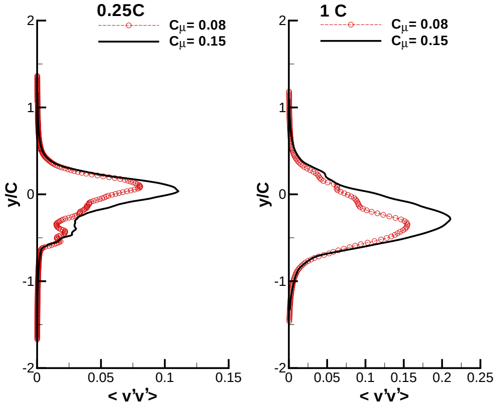

Figure 23: Lateral Reynolds stress of the CFJ airfoil at 30^o AOA predicted by LES